Gas Phase Hydrolysis and Oxo-Exchange of Actinide Dioxide Cations: Elucidating Intrinsic Chemistry from Protactinium to Einsteinium

Monica Vasiliu,[a] John K. Gibson,[b,*] Kirk A. Peterson,[c] and David A. Dixon[a,*]

[a] Department of Chemistry, The University of Alabama, Shelby Hall, Tuscaloosa, Alabama 35487-0336, USA

[b] Chemical Sciences Division, Lawrence Berkeley National Laboratory, Berkeley, California 94720, USA

[c] Department of Chemistry, Washington State University, Pullman WA 99164-4630 USA

[*]Corresponding author email: jkgibson@lbl.gov; dadixon@ua.edu

Abstract

Gas-phase bimolecular reactions of metal cations with water provide insights into intrinsic characteristics of hydrolysis. For the actinide dioxide cations, actinyl(V) AnO_2^+, melding of experiment and computation provides insights into trends for hydrolysis, as well as for oxo-exchange between actinyls and water that proceeds via a hydrolysis pathway. We here extend this line of inquiry farther into the actinide series with CCSD(T) computations of potential energy surfaces for the reaction pathway for oxo-exchange via hydrolysis of nine actinyl(V) ions, from PaO_2^+ to EsO_2^+. The computed surfaces are in accord with previous experimental results for oxo-exchange, and furthermore predict spontaneous exchange for CmO_2^+, BkO_2^+, CfO_2^+ and EsO_2^+, but not for AmO_2^+. Natural Bond Order analysis of the species involved in both hydrolysis and oxo-exchange reveals an inverse correlation between the barrier to hydrolysis and the charge on the actinide center, q(An). Based on this correlation, we conclude that hydrolysis, and related phenomena such as oxo-exchange, become less favorable as the charge on the metal center decreases. The new results provide a straightforward rationalization of trends across a wide swath of the actinide series.

Introduction

Hydrolysis reactions are important in transformations of metal ions and oxides into hydroxides. For actinides (An), these processes impact environmental transport, nuclear fuel processing, and waste treatment and disposition, and it is important to understand the interactions of actinyls with water.[1,2,3,4,5,6,7,8,9,10,11,12,13,14,15] We previously assessed reactions of gas-phase AnO_2^+ with water via oxo-exchange whereby an actinyl oxygen hydrolytically exchanges with that of water. Rios et al.[16] studied exchange of AnO_2^+ (An = U, Np, Pu) by experiment and Kohn-Sham density functional theory (abbreviated as DFT) [17] at the B3LYP /6-311++G(d,p)/Stuttgart-ECP and PBE/TZP-ZORA levels (B3LYP is a hybrid gradient exchange correlation functional, ECP = effective core potential, PBE is a gradient corrected functional, ZORA = Zero-Order Regular Approximation, an approximate relativistic Hamiltonian). Dau et al.[18] extended the experiments to PaO_2^+. We used very high levels of theory (coupled cluster theory with single and double excitations and an approximate triples correction (CCSD(T)) extrapolated to the complete basis set limit plus additional corrections) to predict potential energy surfaces for the for the oxo-exchange via hydrolysis of $AnO_2^{0/+/2+}$ for An = Th(IV)O_2^0, Pa(V)O_2^+, U(V)O_2^+ and U(VI)O_2^{2+},[19] with results in agreement with experiment. Subsequently, the energetics of bare AnO_2^+ and AnO^+ were obtained at the CCSD(T) and complete active space (CAS) levels of theory;[20] predictions included that AnO_2^+ for An = Pa to Lr exhibit a minimum bond dissociation energy (D[(OAn$^+$)-O]) at CmO_2^+. For An = Fm, Md, No and Lr, the predicted most stable AnO_2^+ structure is not linear actinyl(V), $[O=An=O]^+$, but rather side-on bonded An-η^2-$(O_2)^+$, as An(III) peroxides (An = Lr) or An(II) superoxides (An = Fm, Md, No). (We note that an error in the correlated orbitals led to the Cm(III) structure being lower in energy than the actinyl Cm(V) structure. The lowest energy structure is actually the Cm(V) actinyl with ΔE(electronic) = 7 kcal/mol, and by 11 kcal/mol including spin-orbit corrections.) Kaltsoyannis[21] used DFT with the B3LYP functional and pseudo potential basis sets, along with NBO (Natural Bond Orbitals)[22,23,24,25] and QTAIM (Quantum Theory of Atoms in Molecules)[26] bonding analyses, to conclude that, for An = Pa-Pu, reactivity of AnO_2^+ with water correlates with the degree of An-O bond covalency.

We here extend our computational studies at the CCSD(T) level using the most recent all electron basis sets of Peterson and co-workers for the oxo-exchange via hydrolysis of AnO_2^+ for An = Pa to Es. The computational results are assessed in the context of the intertwined phenomena of hydrolysis and oxo-exchange. The AnO_2^+ for An = Pa to Es encompass a range of actinides

(Figure 1) and provide insights into trends across the series. The overarching goals are to assess variations in their reactivity and the underlying basis for these changes to provide additional insights into intrinsic chemistry of the actinides.

		$5f^0$	$5f^1$	$5f^2$	$5f^3$	$5f^4$	$5f^5$	$5f^6$	$5f^7$	$5f^8$				
89	90	91	92	93	94	95	96	97	98	99	100	101	102	103
Ac	Th	Pa	U	Np	Pu	Am	Cm	Bk	Cf	Es	Fm	Md	No	Lr
Actinium	Thorium	Protactinium	Uranium	Neptunium	Plutonium	Americium	Curium	Berkelium	Californium	Einsteinium	Fermium	Mendelevium	Nobelium	Lawrencium

Figure 1. The actinide (An) series of elements, with those of focus here highlighted in red. The formal 5f-orbital occupancy in the AnO_2^+ actinyl(V) cations (i.e., the An^{5+} configuration) is indicated at the top, varying from $5f^0$ for PaO_2^+ (Pa^{5+}) to $5f^8$ for EsO_2^+ (Es^{5+}).

Computational Details

Geometries were optimized and vibrational frequencies were calculated at the DFT level with the B3LYP functional.[27,28] The aug-cc-pVDZ basis sets[29,30] were used for H and O and the Stuttgart large core ECPs and associated basis sets for the actinides.[31] These calculations were done with the Gaussian09 program system.[32]

All-electron single point CCSD(T)[33,34,35,36] calculations using the 3rd-order Douglas-Kroll-Hess Hamiltonian[37,38,39] were performed at the DFT optimized geometries with the aug-cc-pV*n*Z-DK for H,[40] aug-cc-pwCV*n*Z-DK for O[41,42,43] and cc-pwCV*n*Z-DK3 for An[19,57,44] basis sets for *n* = D, T. The CCSD(T) electronic energies were used with the thermal corrections obtained from the DFT calculations to predict thermodynamic properties. The calculations included the correlation of the valence electrons and the An 5s, 5p, 5d, 6s and 6p core-shell electrons and the 1s core-shell electrons of O. The open-shell calculations were done with the R/UCCSD(T) approach where a restricted open shell Hartree-Fock (ROHF) calculation was initially performed and the spin constraint was then relaxed in the coupled cluster calculation.[45,46,47,48] We note that it is very important to carefully examine the orbital occupancies in the valence space and in the 'core' orbitals. For the latter, there can be interleaving orbitals that are not correlated.

We also performed calculations by changing the starting orbitals[19,49,50] for the CCSD(T) calculations from the Hartree-Fock orbitals to Kohn-Sham orbitals from DFT generated using the PW91 generalized gradient exchange-correlation functional.[51,52,53] The reference energy in CCSD arises from diagonalizing the normal HF Hamiltonian with these Kohn-Sham orbitals. Hence no

additional correlation effects are included that are not normally in the CCSD calculation. In all cases the use of PW91 orbitals resulted in much smaller values of the T_1 diagnostic.[54] Thus, these Kohn-Sham orbitals are evidently more optimal than HF for these systems.

The CCSD(T) calculations were performed with the MOLPRO 2015 program package.[55,56] The calculations were performed on our local (UA and WSU) Opteron- and Xeon-based Linux clusters.

Results and Discussion

Potential Energy Surfaces – General Considerations

The essential components of reactions of AnO_2^+ with H_2O are shown on the model potential energy surface (PES) in Scheme 1. With reference to labels in Scheme 1, we consider the following salient attributes of this PES, noting that relative energies depend on the specific identity of An.

(a) The energy of the separated reactants, AnO_2^+ and H_2O, is defined as zero (E ≡ 0). For a bimolecular proton transfer reaction to be observed in an ion trap under the conditions typically used, the energy cannot exceed this so-called reactant asymptote.

(b) Physisorption association of AnO_2^+ and H_2O yields the Lewis acid-base hydrate complex, $(H_2O)AnO_2^+$. The energy for this association reaction is the hydration energy, ΔH(hydrate).

(c) The hydrate can rearrange via the first transition state, TS1, which corresponds to proton transfer from H_2O to one of the axial actinyl O atoms of AnO_2^+. The TS1 barrier is ΔH(TS1), and the energy of TS1 relative to the reactants is E(TS1).

(d) The reaction proceeds via TS1 to yield intermediate $AnO(OH)_2^+$, which is the chemisorption hydrolysis product in which proton transfer is complete. The energy for transformation of hydrate $(H_2O)AnO_2^+$ to hydroxide $AnO(OH)_2^+$ is the hydrolysis energy, ΔH(hydrol).

(e) If present, an asymmetric distorted T-shape intermediate $AnO(OH)_2^+$ can exchange OH positions via TS2, which is a symmetric Y-shape $AnO(OH)_2^+$ with two equivalent hydroxyl groups. If intermediate $AnO(OH)_2^+$ already exhibits a symmetric Y structure, then there is no transition state TS2.

The PES in Scheme 1 is for hydrolysis to yield hydroxide $AnO(OH)_2^+$. Oxo-exchange of $An^{16}O_2^+$ and $H_2{}^{18}O$ occurs via this hydrolysis PES according to Scheme 2. Here, and in exchange experiments, the two O atoms in AnO_2^+ are the naturally dominant (99.8%) O-16 isotope, while the H_2O has been isotopically labelled with O-18. Exchange occurs by association of $An^{16}O_2^+$ with $H_2{}^{18}O$ to yield the hydrate $(H_2{}^{18}O)An^{16}O_2^+$, which hydrolyzes to yield symmetric TS2 hydroxide,

$An^{16}O(^{16}OH)(^{18}OH)^+$, ***(e)*** in Scheme 1. The two hydroxyl O-atoms in TS2 are equivalent; the $An^{16}O^{18}O^+$ exchange product is obtained via the mirror-image of the PES in Scheme 1, to yield $(H_2{}^{16}O)An^{16}O^{18}O^+$ from which physisorbed $H_2{}^{16}O$ is eliminated. Bimolecular oxo-exchange under the ion-molecule reaction conditions usually used cannot occur if any energy on the PES exceeds the reactant asymptote.

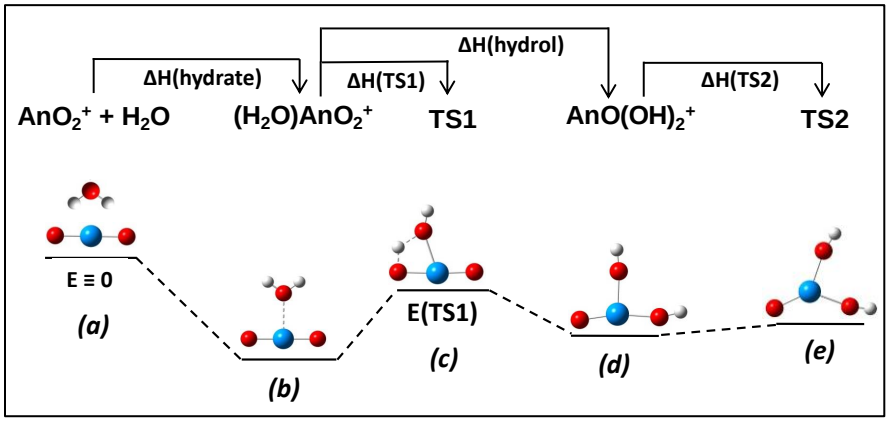

Scheme 1. Generic hydrolysis PES. For An = Pa and Cm there is no TS2 and the structure of the $AnO(OH)_2^+$ intermediate is symmetric as shown for TS2. Indicated energies are for hydration and hydrolysis, ΔH(hydrate) and ΔH(hydrol), TS barriers, ΔH(TS1) and ΔH(TS2), and energy E(TS1). The labels ***(a)-(e)*** refer to the discussion.

Potential Energy Surfaces – Computed Structures and Energies

Key PES energies are given in Table 1, with the CCSD(T)/awT-DK3 (awT is the abbreviation for aug-cc-pVTZ-DK for H, aug-cc-pwCVTZ-DK for O and cc-pwCVTZ-DK3 for An) values for ΔH(hydrate), ΔH(hydrol) and E(TS1) plotted in Figure 2 as a function of actinide. The Lewis acid-base complexes $(H_2O)AnO_2^+$ have C_{2v} symmetry. The C_{2v} hydrate structure with the water hydrogen atoms perpendicular to the AnO_2^+ plane is a transition state for torsion about the An-OH_2 bond and is about 5 kcal/mol higher in energy (See Supporting Information). One OH group in $AnO(OH)_2^+$ is 'axial' and the other is 'equatorial', except for An = Pa and Cm where the OH groups are symmetric and TS2 is absent. Symmetric $PaO(OH)_2^+$ is pyramidal with C_s symmetry; $CmO(OH)_2^+$ has C_{2v} symmetry. Although $EsO(OH)_2^+$ is planar with inequivalent OH groups, no TS2 could be optimized as the PES is very flat.

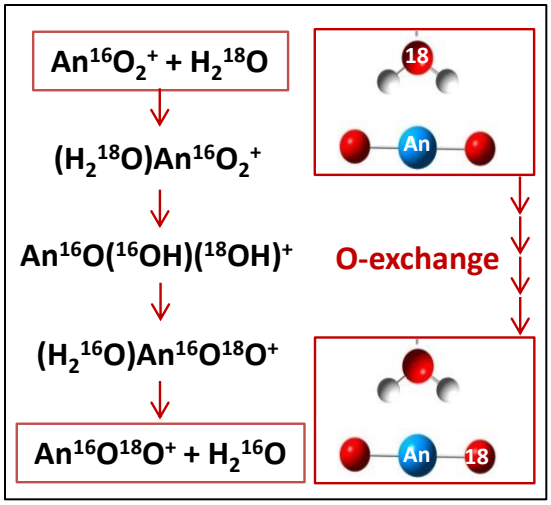

Scheme 2. Steps in oxo-exchange of AnO_2^+ and H_2O, monitored by ^{18}O labeling.

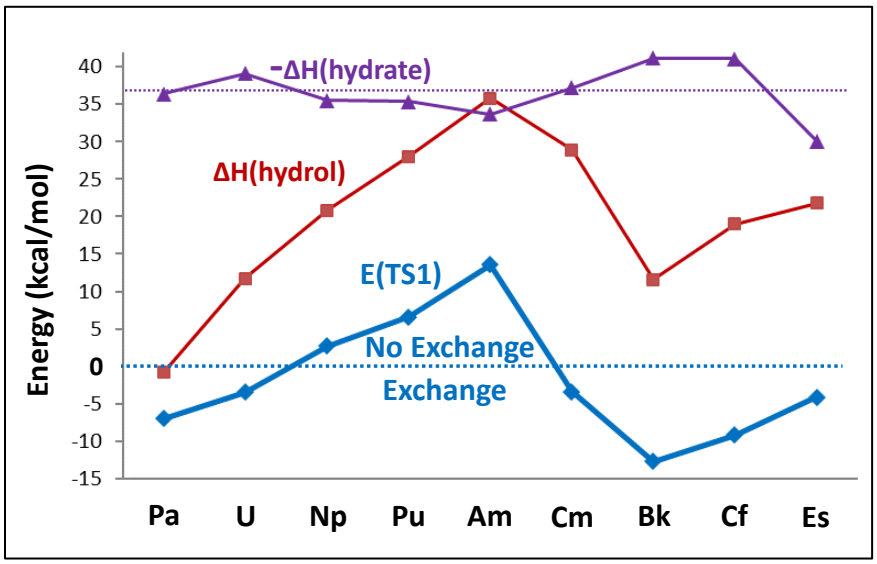

Figure 2. Energies computed at the CCSD(T)/awT-DK3 level. Purple triangles: negative of the hydration enthalpy, -ΔH(hydrate); Red squares: hydrolysis enthalpy, ΔH(hydrol); Blue circles: energy of TS1 relative to the reactant asymptote, E(TS1). The line at zero energy denotes the E(TS1) boundary for oxo-exchange, and that at 37 kcal/mol is close to most of the -ΔH(hydrate).

Table 1. Energies (ΔH_{298} in kcal/mol) for the reaction sequence in Scheme 1.

AnO_2	Method[a]	$E((H_2O)AnO_2^+)$ ≡ ΔH(hydrate)	E(TS1)	$E(AnO(OH)_2^+)$	E(TS2)[b]	ΔH (hydrol)	ΔH (TS1)	ΔH (TS2)
$^1PaO_2^+$	***A***	-36.4	-6.6	-35.8	NB	0.6	29.8	NB
	C	-36.8	-5.6	-34.5	NB	2.3	31.2	NB

	B	-36.4	-7.0	-37.2	NB	-0.8	29.4	NB
	D	-37.7	-7.7	-37.9	NB	-0.2	30.0	NB
	E	-37.3	-7.0	-37.2	NB	0.1	30.3	NB
$^{2}UO_2^+$	***A***	-38.7	-2.0[c]	-24.9	-22.6	13.8	36.7	2.3
	C	-35.0	0.0	-20.1	-19.8	14.9	35.0	0.3
	B	-39.1	-3.5[c]	-27.4	-25.5	11.7	35.6	1.8
	D	-35.9	-1.6	-24.5	-24.5	11.4	34.3	0
	E	-36.1	-1.3	-24.4	-24.0	11.7	34.8	0.4
$^{3}NpO_2^+$	***A***	-35.2	3.9	-12.1	-9.1	23.1	39.1	3.0
	B	-35.5	2.7	-14.7	-12.6	20.8	38.2	2.1
$^{4}PuO_2^+$	***A***	-35.4	8.1	-3.9	4.9	31.5	43.5	8.8
	B	-35.4	6.6	-7.4	0.8	28.0	42.0	8.2
$^{5}AmO_2^+$	***A***	-33.8	15.3	6.6	23.4	40.4	49.1	16.8
	B	-33.7	13.6	2.1	21.2	35.8	47.3	19.1
$^{6}CmO_2^+$	***A***	-37.0	-0.3	-4.5	NB	32.5	36.7	NB
	B	-37.2	-3.4	-8.3	NB	28.9	33.8	NB
$^{7}BkO_2^+$	***A***	-41.0	-11.3	-26.9	-14.6	14.1	29.7	12.3
	B	-41.2	-12.7	-29.6	-16.4	11.6	28.5	13.2
$^{6}CfO_2^+$	***A***	-41.0	-8.2	-19.6	-2.9	21.4	32.8	16.7
	B	-41.1	-9.2	-22.1	-2.4	19.0	31.9	19.7
$^{5}EsO_2^+$	***A***	-30.7	-4.2	-6.1	NB	24.6	26.5	NB
	B	-30.1	-4.1	-8.3	NB	21.8	26.0	NB

[a] ***A*** = CCSD(T)/awT-DK3; ***B*** = CCSD(T)/awT-DK3(PW91); ***C*** = CV-CBS(wCV*n*Z)-DK[19]; ***D*** = CCSD(T)/CBS(awCV*n*Z)-PP(PW91)[19]; ***E*** = CCSD(T)/CBS-PP-DK(PW91)+corrections[19 b]. NB = No Barrier (barrier could not be located for EsO_2^+). [c] For TS1 we used the corrections from B3LYP/aug-cc-pvdz(O,H)/cc-pvdz-PP(Pa,U) optimized geometries.

We previously reported even higher level results for the reactions of H_2O with PaO_2^+ and UO_2^+.[19] For An = Pa, the current CCSD(T)/awT-DK3 results are within 1-2 kcal/mol of those results; the use of different starting orbitals (HF or DFT/PW91) for the CCSD(T) calculations affected these energetics by up to 2 kcal/mol. For An = U, the energy differences from the higher level calculations are up to 5 kcal/mol, with the current results predicting the hydrate as more

strongly bound by 3 - 4 kcal/mol; subsequent energies on the PES track this difference. The use of the Stuttgart ECP and basis set for U led to a non-planar geometry (a planar geometry had 2 imaginary frequencies) for TS1 at the B3LYP level but the planar transition state was lower in energy at the CCSD(T) level. We used the frequencies from a calculation at the B3LYP level with the cc-pVDZ-PP basis sets[57,58,59] which does predict a planar geometry for TS1.

The computed initial complexation energy, ΔH(hydrate), ranges from -30 to -41 kcal/mol, an energy range consistent with a Lewis acid-base interaction of H_2O with a positively charged metal center.[60,61] The ΔH(hydrate) are close to -37 kcal/mol (to within <3 kcal/mol) for PaO_2^+ through CmO_2^+; such near constancy is expected for such a Lewis acid-base interaction. The largest differences are the ΔH(hydrate) values for BkO_2^+ and CfO_2^+ of ca. -41 kcal/mol, and for EsO_2^+ of -30 kcal/mol. The An-OH_2 bond distances, in general, decrease from Pa to Es by about 0.15 Å as expected from the actinide contraction (see Supporting Information). However, this bond distance decrease does not correlate with a decrease in the initial complexation energy showing that there are features other than an electrostatic interaction for the initial hydration step.

As noted previously,[19] conversion of $(H_2O)PaO_2^+$ to $PaO(OH)_2^+$ is nearly thermoneutral (i.e., ΔH(hydrol) ≈ 0). As 5f electrons are added, the relative stability of the dihydroxide decreases, with ΔH(hydrol) increasing to a maximum of ~36 kcal/mol for $AmO(OH)_2^+$ (Figure 2, red squares), then decreasing to ~12 kcal/mol for BkO_2^+ and increasing to ~22 kcal/mol for $EsO(OH)_2^+$.

The initial proton transfer barrier, ΔH(TS1), increases regularly from PaO_2^+ (~30 kcal/mol) to AmO_2^+ (~47 kcal/mol). Thus the barrier height increases with the endothermicity of the reaction, consistent with Hammond's postulate.[62] There is a significant decrease from AmO_2^+ to CmO_2^+ (~34 kcal/mol) and then a decrease to ~26 kcal/mol for EsO_2^+, with CfO_2^+ slightly out of a linear decrease at 32 kcal/mol. The quantity E(TS1) is given by equation (1) and plotted in Figure 2 and

$$E(TS1) = \Delta H(TS1) + \Delta H(hydrate) \quad (1)$$

provides insights into whether a reaction can be observed or not. E(TS1) is below the reactant asymptote for PaO_2^+, UO_2^+, CmO_2^+, BkO_2^+, CfO_2^+, and EsO_2^+, and above it for NpO_2^+, PuO_2^+ and AmO_2^+. In accord with the computations, it has been demonstrated that spontaneous gas-phase oxo-exchange occurs for PaO_2^+ and UO_2^+, but not for NpO_2^+ or PuO_2^+. It is predicted that spontaneous exchange should also occur for CmO_2^+, BkO_2^+, CfO_2^+ and EsO_2^+, but not AmO_2^+. After PuO_2^+, decreasing stabilities of the AnO_2^+ make synthesis increasingly challenging, which,

together with transplutonium isotope scarcity and radioactivity, presents substantial impediments to experimental studies of oxo-exchange. The An=O bond distances in AnO_2^+ and $(H_2O)AnO_2^+$ are given in the Supporting Information. These bond distances are shortest for Pu and Am and the values of E(TS1) are largest here as well suggesting a possible correlation. These bond distances increase and show a larger variation for Cm to Es, as do the values for E(TS1).

Hydrolysis versus Bond Dissociation

As is apparent in Figure 2, the trends in ΔH(hydrol) and E(TS1) are essentially the same. Notable features include distinct maxima for ΔH(hydrol) and E(TS1) at AmO_2^+. The correlation between ΔH(hydrol) and E(TS1) indicates that the key barrier in hydrolysis and exchange is for conversion of an An=O to two An-OH moieties. It might be expected that the barrier to bond disruption in $[O=An=O]^+$ should correlate with the bond dissociation energy, $D[(OAn^+)-O]$. The computed $D[(OAn^+)-O]$ in Table 2, which are plotted in Figure 3 (solid green circles), differ from values in our previous work, which did not have the core orbitals correlated in a consistent manner due to orbital rotation issues in the Douglas-Kroll calculations. Although there are large uncertainties for most experimental $D[(AnO^+)-O]$ (open green circles in Fig. 3), and only lower limits for BkO_2^+ and CfO_2^+, there is generally quite good agreement with predictions; the computations clearly capture the salient trends. The maximum $D[(OAn^+)-O]$ is for PaO_2^+ and the minimum for CmO_2^+. The plots of $D[(OAn^+)-O]$ and ΔH(hydrol) in Figure 3 reveal that there is not a direct correlation between decreasing An=O bond dissociation energy and ease of hydrolysis. Notably, the largest bond dissociation energy and the smallest hydrolysis energy appear for PaO_2^+. Dau et al.[18] surmised that since the impediment to hydrolytic oxo-exchange is not the energy to dissociate an An=O bond, the barrier E(TS1), and the hydrolysis energy ΔH(hydrol), might instead at least partially reflect the degree of bond covalency. Their rationale was that an An=O bond is not cleaved in oxo-exchange or hydrolysis, but a more ionic (less covalent) An=O bond might be more susceptible to transformation to ionic An-OH bonds

Table 2. Experimental and calculated An-O bond dissociation energy ($D[(OAn^+)-O]$) in kcal/mol.

AnO_2	**Experiment**	**CCSD(T) HF / PW91 (awT)ΔH_{298K}**
$^1PaO_2^+$	186 ± 7	202.0 / 203.1
$^2UO_2^+$	177 ± 3	184.9 / 187.5
$^3NpO_2^+$	146 ± 3	161.7 / 165.4

$^{4}PuO_2^+$	122 ± 9	138.4 / 142.4
$^{5}AmO_2^+$	98 ± 13	108.0 / 113.5
$^{6}CmO_2^+$	48 ± 14	63.4 / 68.8
$^{7}BkO_2^+$	≥ 73	84.3 / 87.1
$^{6}CfO_2^+$	≥ 73	69.3 / 72.4
$^{5}EsO_2^+$	-	74.6 / 79.8

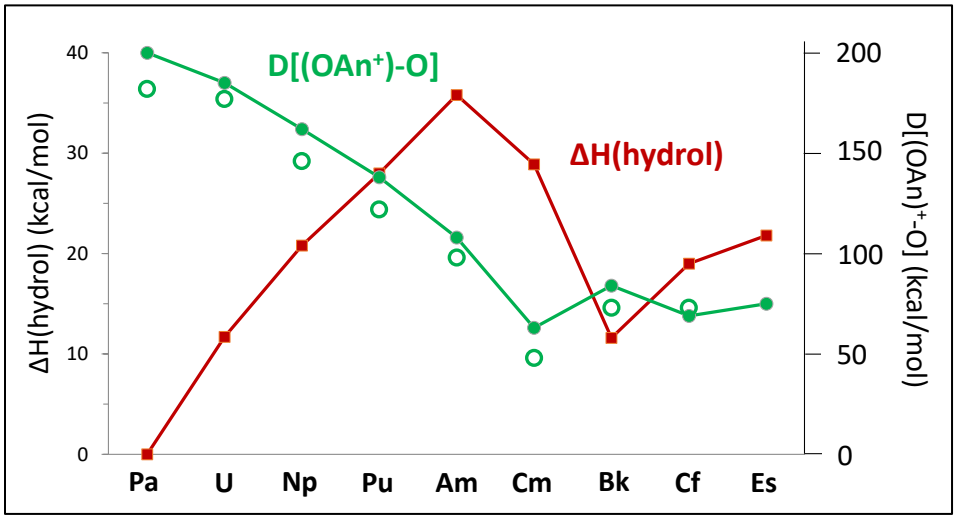

Figure 3. Computed CCSD(T)/awT-DK3(PW91) energies for ΔH(hydrol) (red squares) and D[(OAn$^+$)-O] (solid green circles). Open green circles are experimental D[(OAn$^+$)-O] (lower limits for BkO_2^+ and CfO_2^+).

regardless of D[(OAn$^+$)-O]. This hypothesis was computationally bolstered by Kaltsoyannis[21] with a demonstration that An-O bond covalency increases from PaO_2^+ to PuO_2^+. The present results indicate a maximum in ΔH(hydrol) (and E(TS1)) for AmO_2^+, which could thus suggest a maximum in bond covalency there. Notably, although D[(OAm$^+$)-O] is ~100 kcal/mol less than D[(OPa$^+$)-O], it is predicted that AmO_2^+ should be much more resistant to oxo-exchange than PaO_2^+.

Population analysis

The Natural Population Analysis results based on the Natural Bond Orbitals (NBOs)[63,64] using NBO6[65,66] are given in Table 3 using the B3LYP functional. The NBOs obtained with the PW91 functional are given in Supporting Information. The PW91 NBOs do not differ in any significant way from the B3LYP NBOs. The NBOs for TS1 fall between those of $H_2O(AnO_2)^+$ and $AnO(OH)_2^+$ and are given in the Supporting Information at the B3LYP level. The compositions

of AnO_2^+ and $(H_2O)AnO_2^+$ are approximately $5f^{n+2}6d^1$ where n is the An^{5+} $5f^n$ occupancy in Figure 1 (n=0 for Pa, n= 1 for U, etc.). The 5f occupancy decreases by ca. 0.2-0.4 e from a given $(H_2O)AnO_2^+$ to the corresponding $AnO(OH)_2^+$.

Table 3. NBO6 populations at B3LYP/aug-cc-pvdz(O,H)/Stuttgart(An) level using B3LYP/ aug-cc-pvdz(O,H)/Stuttgart(An) optimized geometries.

Molecule	**Property**[a]	**Pa**	**U**	**Np**	**Pu**	**Am**	**Cm**	**Bk**	**Cf**	**Es**
AnO_2^+	q(An)	2.49	2.34	2.20	2.09	2.00	2.13	2.30	2.27	2.24
$(H_2O)AnO_2^+$	q(An)	2.44	2.27	2.13	2.02	1.94	2.08	2.25	2.22	2.18
$AnO(OH)_2^+$	q(An)	2.62	2.43	2.28	2.15	2.13	2.28	2.33	2.31	2.27
AnO_2^+	5f Total	1.82	2.98	4.16	5.31	6.43	7.30	8.08	9.13	10.24
$(H_2O)AnO_2^+$	5f Total	1.77	2.94	4.11	5.28	6.39	7.25	8.03	9.08	10.18
$AnO(OH)_2^+$	5f Total	1.24	2.66	3.83	5.01	6.07	6.99	7.84	8.91	10.02
AnO_2^+	5f Excess	1.82	1.98	2.16	2.31	2.43	2.30	2.08	2.13	2.24
$(H_2O)AnO_2^+$	5f Excess	1.77	1.94	2.11	2.28	2.39	2.25	2.03	2.08	2.18
$AnO(OH)_2^+$	5f Excess	1.24	1.66	1.83	2.01	2.07	1.99	1.84	1.91	2.02
AnO_2^+	5fα	0.91	2.02	3.15	4.29	5.45	6.34	6.80	6.81	6.82
	5fβ	0.91	0.96	1.01	1.02	0.98	0.96	1.28	2.32	3.42
$(H_2O)AnO_2^+$	5fα	0.89	2.00	3.14	4.27	5.42	6.32	6.80	6.81	6.82
	5fβ	0.89	0.94	0.97	1.01	0.97	0.93	1.23	2.27	3.37
$AnO(OH)_2^+$	5fα	0.62	1.85	2.99	4.17	5.36	6.69	6.84	6.84	6.85
	5fβ	0.62	0.81	0.84	0.83	0.71	0.30	1.01	2.07	3.17
AnO_2^+	6d	0.93	0.90	0.90	0.86	0.81	0.79	0.84	0.82	0.78
$(H_2O)AnO_2^+$	6d	0.99	0.97	0.93	0.92	0.86	0.85	0.91	0.89	0.86
$AnO(OH)_2^+$	6d	1.23	1.02	1.02	0.97	0.91	0.77	0.93	0.90	0.85

[a]5f Excess is the additional 5f population over An^{5+} $5f^n$ (n=0 for Pa, n=1 for U, etc.).

The An 6d population plotted in Figure 4 generally exhibits a gradual decrease across the series. The increase in 6d population from AnO_2^+ to $(H_2O)AnO_2^+$ is consistent with a Lewis acid-base interaction, with charge donation from H_2O to An 6d. Except for Cm, the 6d population further increases from $(H_2O)AnO_2^+$ to $AnO(OH)_2^+$; there is no significant 6d population difference for $(H_2O)AnO_2^+$ versus $AnO(OH)_2^+$ for Bk, Cf and Es. An effect that is apparent for all three Cm complexes, a drop in 6d relative to other An, is particularly extreme for $CmO(OH)_2^+$ where 5fβ is also anomalously low while 5fα is correspondingly high such that 5fα-5fβ is 6.39 (values in Table 3). This quantity 5fα-5fβ represents the unpaired 5f population, and for Cm it approaches that of a particularly stable half-filled shell $5f^7$ configuration.

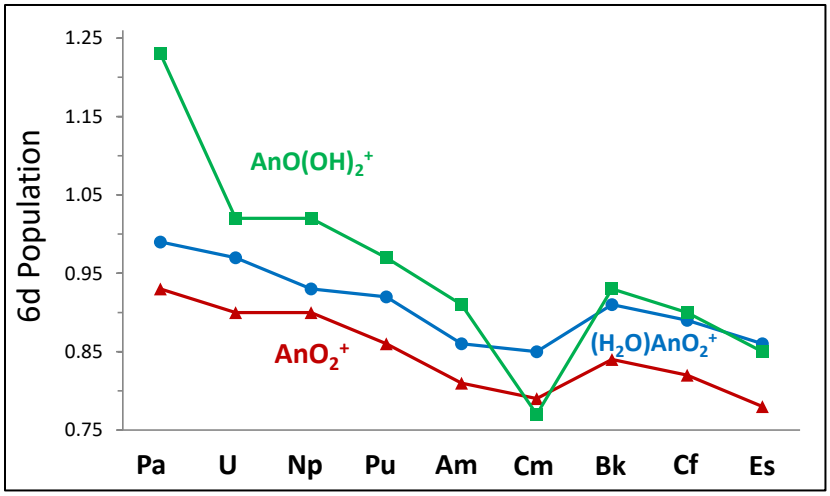

Figure 4. NBO 6d population in AnO_2^+ (red triangles), $(H_2O)AnO_2^+$ (blue circles) and $AnO(OH)_2^+$ (green squares).

The quantity '5f Excess' derived from the NBOs is here defined as the additional 5f population above that for a bare An^{5+} ion, and it thus corresponds to the 5f population due to back-donation to the formal $5f^n$ An^{5+} core (Figure 5). Although "An^{5+}" is an artificial, although not arbitrary, formal construct, the same trends appear if any different atomic charge state, such as neutral An^0, is employed. While 5f Excess is the reduction in charge on formally $5f^n$ An^{5+} due to donation into 5f, the total charge reduction is given by '5f Excess + 6d', which is plotted in Figure 6. From Figures 5 and 6 it is apparent that both '5f Excess' and '5f Excess + 6d' exhibit maxima at Am, and that there is a correlation between these NBO parameters and the ΔH(hydrol) plotted in Figure 2. This correlation may suggest increasing resistance to hydrolysis, and oxo-exchange, as a result of increasing net backdonation from oxygen to 5f and 6d of An(V). As such backdonation essentially represents sharing of electron density between An and O, it can be considered as increasing bond "covalency", or equivalently as increasing "ionicity". In the extreme ionic limit AnO_2^+ would be hypothetical $(An^{5+})(O^{2-})_2$ with 5f Excess = 6d = 0. Our population analysis thus indicates that total An-O bond covalency, and the 5f contribution to it, both increase from PaO_2^+ to AmO_2^+, which is in full accord with the assessment by Kaltsoyannis[21] who identified an increase in covalency from PaO_2^+ to PuO_2^+.

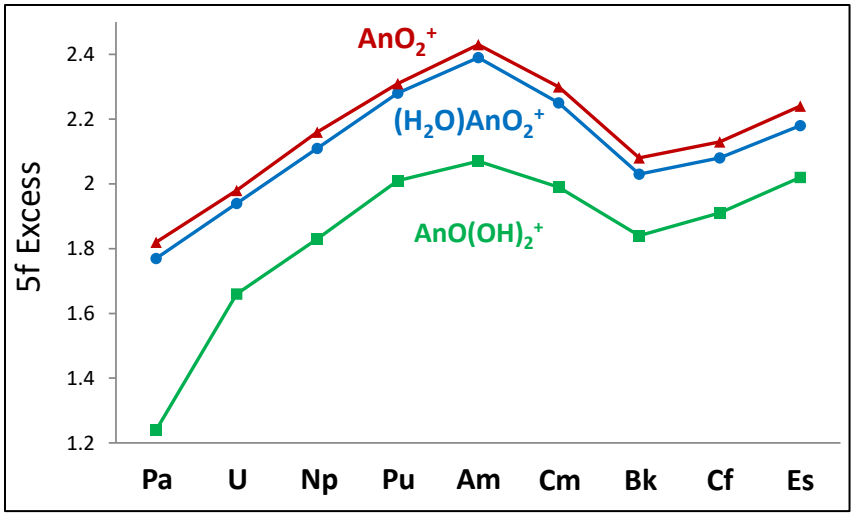

Figure 5. NBO '5f Excess' for AnO_2^+ (red triangles), $(H_2O)AnO_2^+$ (blue circles) and $AnO(OH)_2^+$ (green squares). '5f Excess' is the excess 5f population as compared with An^{5+}.

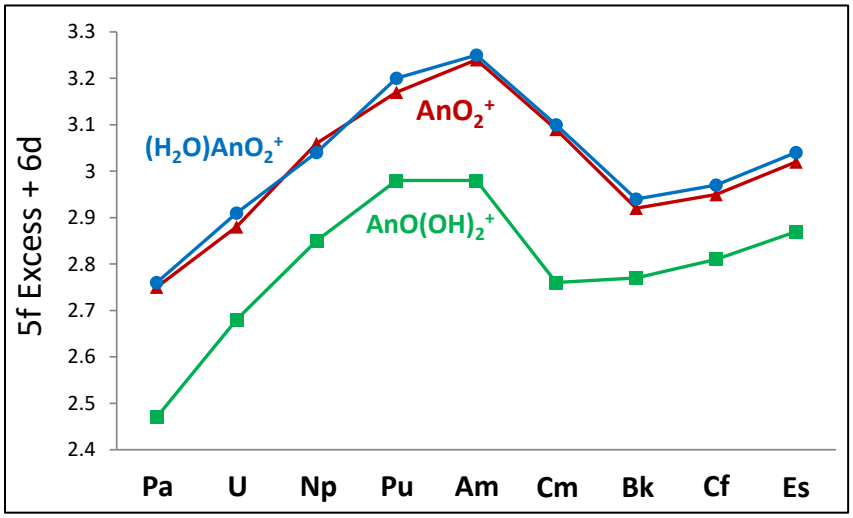

Figure 6. Sum of '5f Excess' and 6d populations in AnO_2^+ (red triangles), $(H_2O)AnO_2^+$ (blue circles) and $AnO(OH)_2^+$ (green squares).

As an alternative to the notion of "covalency", we consider the NBO parameter q(An), the charge on An, which is plotted in Figure 7. It is not proposed that these q(An) represent a physical charge, but rather that they reveal comparative charges for different compositions and different An. As expected, q(An) generally inversely correlates with '5f Excess + 6d' (Figure 6), which is the charge donation to a formal An^{5+} ($q \equiv 5$). The close correlation between Fig. 6 and Fig. 7, particularly for the simple case of bare AnO_2^+ (red points), implies that the excess charge relative to An^{5+} is mostly in 5f and 6d orbitals, with little population in other orbitals such as 7s. The variations in q(An) between the three types of species are reasonable. Association of water to bare

AnO_2^+ results in Lewis base charge donation and a small decrease in q(An) for $(H_2O)AnO_2^+$. Formation of another discrete An-O bond in $AnO(OH)_2^+$ results in charge-withdrawal into the third new An-O bond and an increase in q(An).

Comparison of Figures 2 and 7 reveals an inverse correlation between ΔH(hydrol) and q(An) for all three species, including $(H_2O)AnO_2^+$. This correlation, presented more explicitly in Figure 8, suggests that higher q(An) somehow facilitates hydrolysis, and that essential features of the PES in Figure 2 are related to the charge on the actinide center. It is presumably the An charge density, ρ_q, that should govern ionic interactions. As ionic radii decrease across the series due to the actinide contraction, ρ_q increases. However, it is not practical to assign an ionic radius for an extremely non-spherical actinyl. Furthermore, it is unwarranted to employ either a simple surface or volume charge density, even if some sort of effective radius could reasonably be assigned. Fortunately, the gradual decrease in effective radii from PaO_2^+ to EsO_2^+ will not alter trends in ρ_q as indicated by q(An).

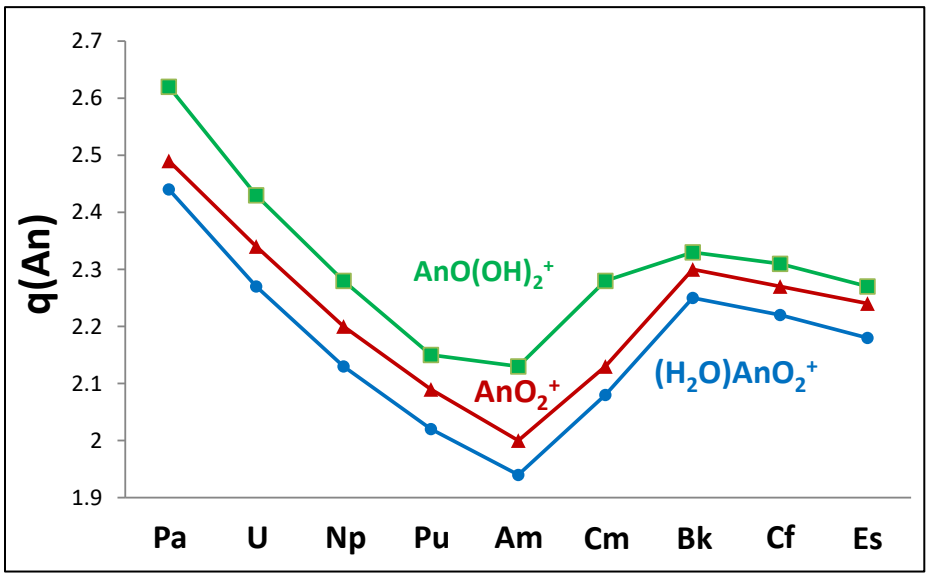

Figure 7. NBO Charge q(An) for AnO_2^+ (red triangles), $(H_2O)AnO_2^+$ (blue circles) and $AnO(OH)_2^+$ (green squares).

Comparison of Figures 4-7 reveal that the variation in q(An) is due mostly to '5f Excess', which peaks at AmO_2^+. As nuclear charge Z increases, donation into An 5f should become more favorable, as happens from Pa to Am. Between Am and Cm, '5f Total' increases to ≥7 e such that additional 5f population must go into partially occupied 5f orbitals beginning at Cm. Beyond the

half-filled $5f^7$ configuration around Am(V), the energy advantage for donation into the 5f is thus diminished by electron-electron repulsion, which might explain why '5f Excess' is a maximum and q(An) a minimum at Am. As remarked above, decreasing q(An), which corresponds to increasing charge donation from oxygen, can alternatively be considered as increasing bond covalency and decreasing ionicity.

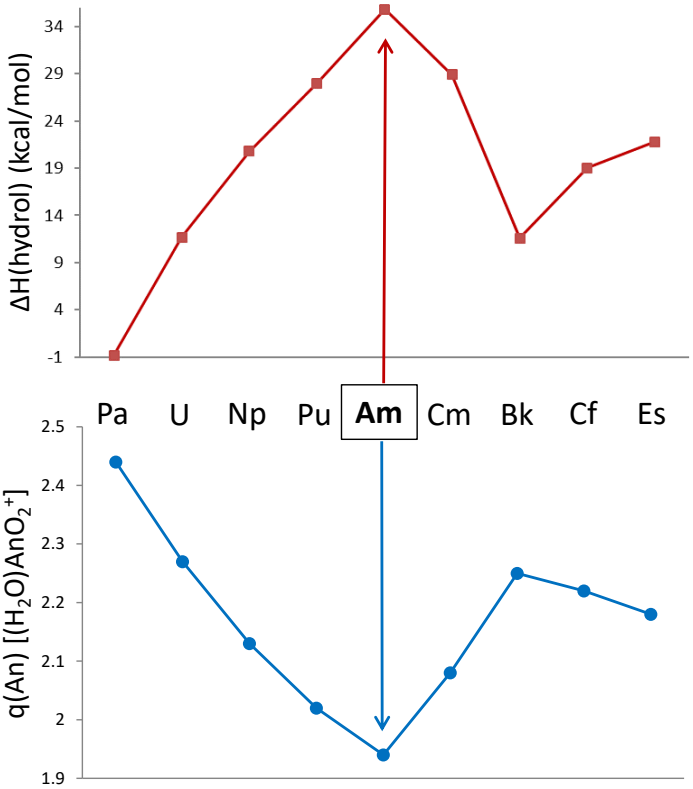

Figure 8. ΔH(hydrol) (Top) and q(An) for $(H_2O)AnO_2^+$ (Bottom).

As shown in the Supporting Information, the amount of excess α spin on the actinide in the AnO_2^+ peaks at Cm and Bk (the amount of excess spin on the An in the $(H_2O)AnO_2^+$ complex essentially falls on the same line). The peak in E(TS1) is at Am showing that the amount of excess α spin on the An is a possible contributing factor but not the only one. There is some spin polarization in the starting AnO_2^+ and in the $(H_2O)AnO_2^+$ complex with excess β spin on the actinyl oxygen (see Supporting Information). The largest amount of spin polarization is found for An = Am (~0.25 β) and this is where the largest value of E(TS1) is found. Although the spin polarization for An = Cm is only slightly smaller for Cm as compared to Am, there is a significant change in E(TS1). For An = Cf, Bk, or Es, there is no spin polarization on the actinyl oxygen atoms as these

atoms have excess α spin. The species with excess α spin have a negative value for E(TS1). These results point to the fact that the amount of spin polarization is a potential contributing factor to the value of E(TS1). The values of S^2 are shown in the Supporting Information and the DFT/B3LYP values are consistent with the CCSD(T) values. The largest deviations are found for An = Cm with the dihydroxide always having the largest deviation for a given actinide.

A key attribute of the correlations identified here is that no direct causal relationship need be assigned. It is however appealing to consider possible relevant factors. The initial proton transfer barrier TS1, as well as O-H bonding in $AnO(OH)_2^+$ (Scheme 1), should generally be facilitated by negative charge on O atoms. Since q(O) is more negative and favorable for higher positive q(An), the decrease in q(An) from Pa to Am should mostly result in destabilization to higher energies of both TS1 and $AnO(OH)_2^+$, which is as predicted from our computational energetic results.

The hydration enthalpies are approximately constant until Bk and Cf, where they become more negative by ca. 4 kcal/mol. From Cf to Es, ΔH(hydrate) becomes substantially less negative, increasing from -41 to -30 kcal/mol. Comparison of ΔH(hydrate) in Figure 2 and q(An) in Figure 7 shows the absence of a distinct correlation such as would be expected for the idealistic situation of only ionic interactions between H_2O and AnO_2^+. The charge on the An undoubtedly does play a role in governing ΔH(hydrate) but it is clearly not the only relevant factor. Among possible other effects, Es(V) is formally $5f^8$ and our analysis yields a configuration around $5f^{10}$; multiple paired 5f electrons might result in increased electron repulsion and reduced electrostatic interaction.

A second order perturbation theory energy analysis[23,24] of the NBOs was performed which examines all possible interactions between donor Lewis-type NBOs (i) and acceptor non-Lewis NBOs (j). The stabilization energy associated with delocalization from i → j is given by $E(2) = q_i(F(i,j)^2/(\varepsilon_i - \varepsilon_j)$ where q_i is the donor orbital occupancy, ε_x are orbital energies, and F(i,j) is the off-diagonal NBO Fock matrix element. These values are given in the Supporting Information for $(H_2O)AnO_2^+$. As expected, the largest energy stabilization is for the two inequivalent lone pairs on the oxygen on the H_2O moiety donating into virtual d and f orbitals on the An. We provide a brief description for the closed shell system Pa as the open shell nature of the remaining complexes significantly complicates the analysis. The most important contribution for the pure 2p lone pair on O is donation into a Pa orbital with $6d^{0.7}5f^{0.3}$ character. The O lone pair with s and p character donates into two orbitals on the Pa, one with $7s^{0.5}6d^{0.4}5f^{0.1}$ character and the other with

$7s^{0.4}6d^{0.5}5f^{0.1}$ character. There are also smaller interactions of the lone pair on O with s and p character with antibonding Pa=O orbitals which are mostly on the Pa and have about equal 6d and 5f character.

Finally, to holistically assess core aspects of the potential energy surface in Scheme 1 we consider the relationship between the transition state barrier, ΔH(TS1), and the hydrolysis energy, ΔH(hydrol). These are plotted together in Figure 9, along with the difference:

$$\Delta\Delta H = \Delta H_{REV}(TS1) = \Delta H(TS1) - \Delta H(hydrol), \quad (2)$$

which is the "reverse" barrier $\Delta H(AnO(OH)_2^+ \rightarrow TS1)$ that we denote as $\Delta H_{REV}(TS1)$. The energy relationships between hydrate $(H_2O)AnO_2^+$, hydroxide $AnO(OH)_2^+$, and TS1 that links them, is shown at the top of Figure 9. For Pa, the hydrate and hydroxide are nearly degenerate in energy, i.e., $\Delta H(hydrol) \approx 0$, and $\Delta H(TS1) \approx \Delta H_{REV}(TS1)$. Between Pa and Am, ΔH(TS1) increases while $\Delta H_{REV}(TS1)$ decreases, a relationship that reflects a drastic corresponding increase in ΔH(hydrol). After Am, the variations and relationships between these three parameters becomes more irregular. The information in Figure 9 is included to emphasize that it is not expected that any single property, q(An) or otherwise, should effectively account for all aspects of the potential energy surface.

The specific correlation between ΔH(hydrol) and q(An) shown in Figure 8 is particularly striking and convincing. We propose that there is a relationship between these parameters, while emphasizing that this does not establish cause-and-effect, and does not exclude correlations with other properties such as bond covalency. An important aspect of relationships such as revealed in Figure 9 is the necessity to study several members of the actinide series. Considering only the five actinides from Pa to Am would suggest a good correlation between ΔH(TS1), $\Delta H_{REV}(TS1)$ and ΔH(hydrol), as well as between all three and q(An). It is the results for Cm and beyond that reveal the failing of these inclusive correlations and indicate a consistently good correlation between ΔH(hydrol) and q(An). It should be noted that because the predominant trends for ΔH(TS1) are similar to those for ΔH(hydrol), there is also a generally good correlation between ΔH(TS1) and q(An).

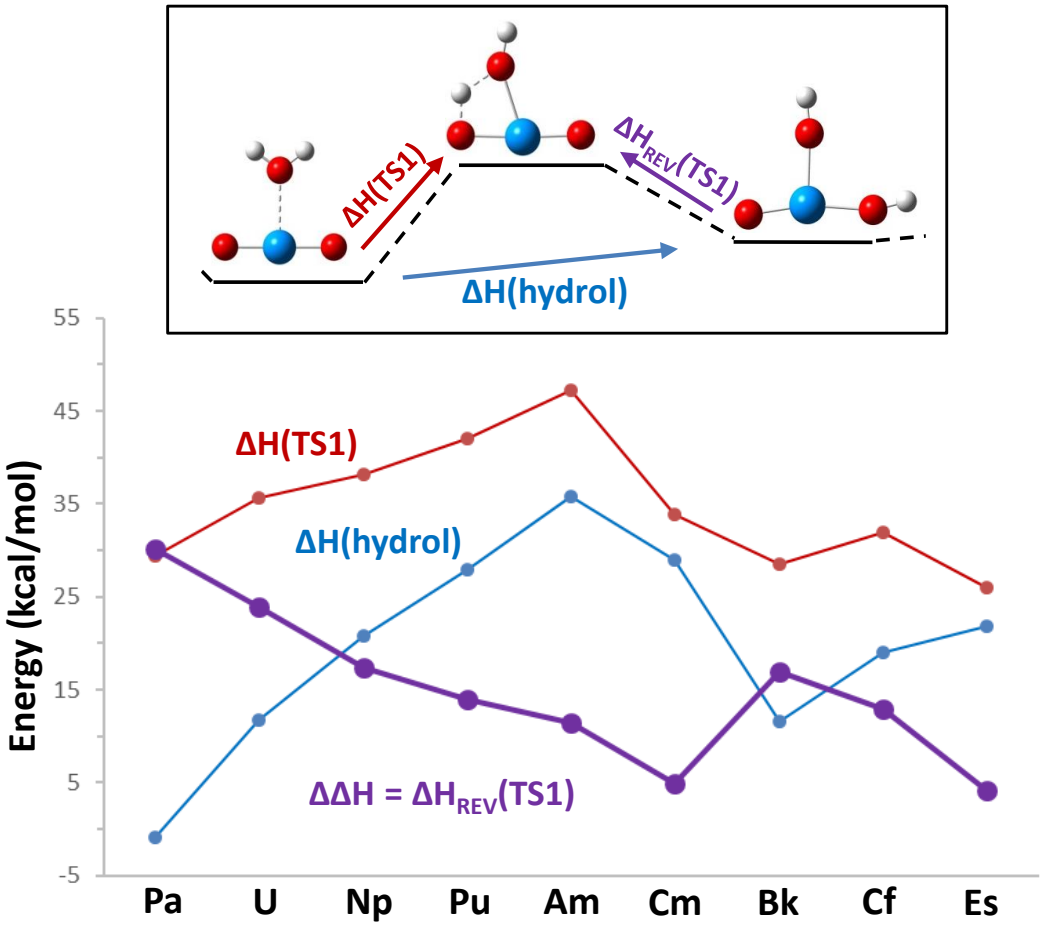

Figure 9. ΔH(hydrol) (red), ΔH(TS1) (blue), and the difference ΔΔH = ΔH(TS1) - ΔH(hydrol) = $\Delta H_{REV}(AnO(OH)_2^+ \rightarrow TS1)$ (purple). The relationship between three energy parameters is shown on the partial potential energy surface at the top.

Conclusions

The potential energy surfaces for adding H_2O to AnO_2^+ followed by a proton transfer, the first step in the hydrolysis of the AnO_2^+ were calculated at the CCSD(T) level with a large basis set including scalar relativistic effects. The computations predict that E(TS1) is below the reactant asymptote of $AnO_2^+ + H_2O$ for An = Pa, U, Cm, Bk, Cf, and Es, and above it for Np, Pu, and Am. Although the An-OH_2 bond distances in the initial hydration complex do correlate with the expected actinide contraction, the initial hydration energies do not correlate with this trend showing that simple electrostatics is not the only effect. The computational results are in agreement with available experimental information, particularly those for gas-phase oxo-exchange of PaO_2^+ to PuO_2^+. As predictions now extend to EsO_2^+, it is desirable to similarly expand experiments and

further assess the validity of the computational results and the correlation. The disconnect between bond dissociation energy D[(OAn^+)-O] and transformation of An=O bonds via hydrolysis, should be further assessed. In particular, AmO_2^+ is predicted to not exhibit oxo-exchange despite that bond dissociation energy D[(OAm^+)-O] is about half D[(OPa^+)-O]. Computational results for transplutonium actinides provide insights into intrinsic chemistry and trends that may remain experimentally inaccessible. For example, it is predicted that hydrolysis properties should be similar for uranyl(V) and berkelyl(V).

An assessment of NBO parameters has enabled a satisfactory rationalization of the observed trends in hydrolysis and oxo-exchange of AnO_2^+. The diminishment in the facileness of hydrolysis of AnO_2^+ is accordant with computed charges on the actinide centers in these species. Greater electron donation from oxo ligands to An results in a reduced charge and less effective bonding with ionic OH ligands, which should generally destabilize hydroxide products, as well as hydroxyl intermediates. Our assessment does not quantify covalency but we do find a decrease in q(An) from PaO_2^+ to AmO_2^+, which corresponds to increasing charge donation from O to An and is thus essentially in accord with the report by Kaltsoyannis[21] of increasing covalency from PaO_2^+ to PuO_2^+. Our results are not whatsoever in contradiction with those of Kaltsoyannis,[21] but assessment for additional heavier AnO_2^+ does reveal a broader correlation with q(An). Without excluding the possibility of effects beyond q(An), and in accord with Ockham's razor, we now adopt the more general and straightforward relationship to understand overall trends from PaO_2^+ to EsO_2^+.

Acknowledgements

J.K.G. was supported by the U.S. Department of Energy, Office of Basic Energy Sciences, Chemical Sciences, Geosciences, & Biosciences Division, Heavy Element Chemistry Program, at LBNL under Contract No. DE-AC02-05-CH11231. D.A.D. acknowledges the support of U.S. DOE, OBES, Heavy Element Chemistry Program. D.A.D. thanks the Robert Ramsay Fund at the University of Alabama. K.A.P. acknowledges the support of the U.S. DOE, OBES, HEC through Grant No. DE-FG02-12ER16329.

Table of Contents

Actinyl oxo-exchange is quintessential bond activation yet is remarkably and enigmatically independent of actinide-oxygen dissociation energy. CCSD(T) computations and Natural Bond Order analysis for nine actinyl(V) ions rationalize the enigma, demonstrating a correlation between exchange efficiency and actinide charge. This charge is a manifestation of 5f orbital filling, such that oxo-exchange reveals essential actinide character.

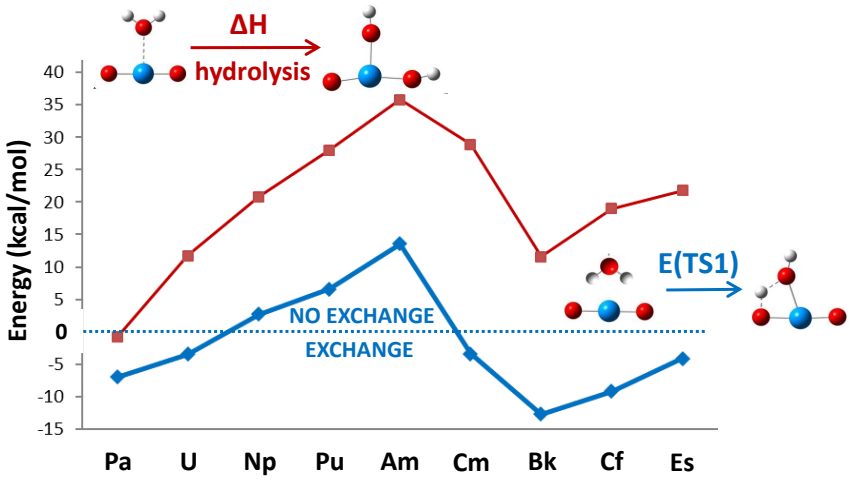

Keywords: Actinides, Transuranium elements, Computational chemistry, Ion-molecule reactions, Reaction mechanisms

References

[1] Crandall, H. W. The Formula of Uranyl Ion. *J. Chem. Phys.* **1949**, *17*, 602−606.

[2] Gordon, G.; Taube, H. J. The Uranium(V)-Catalysed Exchange Reaction Between Uranyl Ion and Water in Perchloric Acid Solution. *Inorg. Nucl. Chem.* **1961**, *16*, 272−278.

[3] Clark, D. L.; Conradson, S. D.; Donohoe, R. J.; Keogh, D. W.; Morris, D. E.; Palmer, P. D.; Rogers, R. D.; Tait, C. D. Chemical Speciation of the Uranyl Ion under Highly Alkaline Conditions. Synthesis, Structures, and Oxo Ligand Exchange Dynamics. *Inorg. Chem.* **1999**, *38*, 1456−1466.

[4] Szabo, Z.; Grenthe, I. Reactivity of the "yl"-Bond in Uranyl(VI) Complexes. 1. Rates and Mechanisms for the Exchange between the *trans*-dioxo Oxygen Atoms in $(UO_2)_2(OH)_2^{2+}$ and Mononuclear $UO_2(OH)_n^{2-n}$ Complexes with Solvent Water. *Inorg. Chem.* **2007**, *46*, 9372−9378.

[5] Szabo, Z.; Grenthe, I. On the Mechanism of Oxygen Exchange Between Uranyl(VI) Oxygen and Water in Strongly Alkaline Solution as Studied by ^{17}O NMR Magnetization Transfer. *Inorg. Chem.* **2010**, *49*, 4928−4933.

[6] Fortier, S.; Hayton, T. W. Oxo Ligand Functionalization in the Uranyl Ion (UO_2^{2+}). *Coord. Chem. Rev.* **2010**, *254*, 197−214.

[7] Wahlin, P.; Danilo, C.; Vallet, V.; Réal, F.; Flament, J. P.; Wahlgren, U. An Investigation of the Accuracy of Different DFT Functionals on the Water Exchange Reaction in Hydrated Uranyl(VI) in the Ground State and the First Excited State. *J. Chem. Theory Comput.* **2008**, *4*, 569−577.

[8] Réal, F.; Vallet, V.; Wahlgren, U.; Grenthe, I. Ab Initio Study of the Mechanism for Photoinduced Yl-Oxygen Exchange in Uranyl(VI) in Acidic Aqueous Solution. *J. Am. Chem. Soc.* **2008**, *130*, 11742−11751.

[9] Shamov, G. A.; Schreckenbach, G. Theoretical Study of the Oxygen Exchange in Uranyl Hydroxide. An Old Riddle Solved? *J. Am. Chem. Soc.* **2008**, *130*, 13735−13744.

[10] Schreckenbach, G.; Shamov, G. A. Theoretical Actinide Molecular Science. *Acc. Chem. Res*. **2010**, *43*, 19−29.

[11] Bühl, M.; Schreckenbach, G. Oxygen Exchange in Uranyl Hydroxide via Two "Nonclassical" Ions. *Inorg. Chem*. **2010**, *49*, 3821−3827.

[12] Bühl, M.; Wipff, G. Insights into Uranyl Chemistry from Molecular Dynamics Simulations. *ChemPhysChem*, **2011**, *12*, 3095−3105.

[13] Tsushima, S. "yl"-Oxygen Exchange in Uranyl(VI) Ion: A Mechanism Involving $(UO_2)_2(\mu\text{-}OH)_2^{2+}$ via $U–O_{yl}–U$ Bridge Formation. *Inorg. Chem*. **2012**, *51*, 1434−1439.

[14] Rabideau, S. W.; Masters, B. J. Oxygen Exchange Reactions of Plutonium Ions in Solution. *J. Phys. Chem*. **1963**, *67*, 318−323.

[15] Rabideau, S. W. The Oxygen Exchange Reactions of NpO_2^{+2} and NpO_2^{+} with Water. *J. Phys. Chem.* **1963**, *67*, 2655−2659.

[16] Rios, D.; Michelini, M. d. C.; Lucena, A. F.; Marçalo, J.; Gibson J. K. On the Origins of Faster Oxo Exchange for Uranyl(V) versus Plutonyl(V). *J. Am. Chem. Soc.* **2012**, *134*, 15488−15496.

[17] Parr, R. G.; Yang, W., *Density-Functional Theory of Atoms and Molecules*. Oxford University Press: New York, 1989.

[18] Dau, P. D.; Wilson, R. E.; Gibson J. K. Elucidating Protactinium Hydrolysis: The Relative Stabilities of $PaO_2(H_2O)^+$ and $PaO(OH)_2^+$. *Inorg. Chem.* **2015**, *54*, 7474–7480.

[19] Vasiliu, M.; Peterson, K. A.; Gibson, J. K.; Dixon, D. A. Reliable Potential Energy Surfaces for the Reactions of H_2O with ThO_2, PaO_2^+, UO_2^{2+}, and UO_2^+. *J. Phys. Chem. A*, **2015**, *119*, 11422−11431

[20] Dau, P. D.; Vasiliu, M.; Peterson, K. A.; Gibson, J. K.; Dixon, D. A. Remarkably High Stability of Late Actinide Dioxide Cations: Extending Chemistry to Pentavalent Berkelium and Californium. *Chem. Eur. J.* **2017** *23*, 17369-17378.

[21] Kaltsoyannis, N. Covalency hinders $AnO_2(H_2O)^+ \rightarrow AnO(OH)_2^+$ isomerisation (An = Pa–Pu). *Dalton Trans.* **2016**, *45*, 3158–3162.

[22] Glendening, E. D.; Landis, C. R.; Weinhold, F. NBO 6.0: Natural Bond Orbital Analysis Program. *J. Comp. Chem*. **2013**, *34*, 1429-1437.

[23] Weinhold, F. Natural Bond Orbital Methods. in *Encyclopedia of Computational Chemistry*; P. v. R. Schleyer, Ed.; John Wiley & Sons: Chichester, U.K., 1998; Vol. 3, pp 1792−1811.

[24] Weinhold, F.; Landis, C. R. *Valency and Bonding: A Natural Bond Orbital Donor-Acceptor Perspective*; University Press: Cambridge, U.K., 2003.

[25] Reed, A. E.; Curtiss, L. A.; Weinhold, F. Intermolecular Interactions from a Natural Bond Orbital, Donor-Acceptor Viewpoint. *Chem. Rev.* **1988**, *88*, 899−926.

[26] Bader, R. F. W. *Atoms in Molecules: A Quantum Theory*, Clarendon Press, Oxford, 1990

[27] Becke, A. D.: Density-Functional Thermochemistry. III. The Role of Exact Exchange. *J. Chem. Phys.* **1993**, *98*, 5648-5652.

[28] Lee, C.; Yang, W.; Parr, R. G., Development of the Colle-Salvetti Correlation-Energy Formula Into a Functional of the Electron Density. *Phys. Rev. B* **1988**, *37*, 785-789.

[29] Dunning, T.H., Jr. Gaussian basiss set for use in correlated molecular calculations. I. The atoms boron through neon and hydrogen. *J. Chem. Phys*. **1989**, *90*, 1007-1023.

[30] Kendall, R. A.; Dunning, T. H., Jr.; Harrison, R. J. Electron Affinities of the First-Row Atoms Revisited. Systematic Basis Sets and Wave Functions. *J. Chem. Phys*. **1992**, *96*, 6796-6806.

[31] Kuchle, W.; Dolg, M.; Stoll, H.; Preuss, H., *J. Chem. Phys.* **1994,** 100, (10), 7535-7542.

[32] Frisch, M. J.; Trucks, G. W.; Schlegel, H. B.; Scuseria, G. E.; Robb, M. A.; Cheeseman, J. R.; Scalmani, G.; Barone, V.; Mennucci, B.; Petersson, G. A.; Nakatsuji, H.; Caricato, M.; Li, X.; Hratchian, H. P.; Izmaylov, A. F.; Bloino, J.; Zheng, G.; Sonnenberg, J. L.; Hada, M.; Ehara, M.; Toyota, K.; Fukuda, R.; Hasegawa, J.; Ishida, M.; Nakajima, T.; Honda, Y.; Kitao, O.; Nakai, H.; Vreven, T.; Montgomery, J. A., Jr.; Peralta, J. E.; Ogliaro, F.; Bearpark, M.; Heyd, J. J.; Brothers, E.; Kudin, K. N.; Staroverov, V. N.; Kobayashi, R.; Normand, J.; Raghavachari, K.; Rendell, A.; Burant, J. C.; Iyengar, S. S.; Tomasi, J.; Cossi, M.; Rega, N.; Millam, J. M.; Klene, M.; Knox, J. E.; Cross, J. B.; Bakken, V.; Adamo, C.; Jaramillo, J.; Gomperts, R.; Stratmann, R. E.; Yazyev, O.; Austin, A. J.; Cammi, R.; Pomelli, C.; Ochterski, J. W.; Martin, R. L.; Morokuma, K.; Zakrzewski, V. G.; Voth, G. A.; Salvador, P.; Dannenberg, J. J.; Dapprich, S.; Daniels, A. D.;

Farkas, O.; Foresman, J. B.; Ortiz, J. V.; Cioslowski, J.; Fox, D. J. Gaussian09, Revision E.01. Gaussian, Inc., Wallingford, CT, 2009.

[33] Purvis, G. D., III; Bartlett, R. J. A Full Coupled-Cluster Singles and Doubles Model: The Inclusion of Disconnected Triples. *J. Chem. Phys.* **1982**, *76*, 1910-1918.

[34] Raghavachari, K.; Trucks, G. W.; Pople, J. A.; Head-Gordon, M. A Fifth-order Perturbation Comparison of Electron Correlation Theories. *Chem. Phys. Lett.* **1989**, *157*, 479-483.

[35] Watts, J. D.; Gauss, J.; Bartlett, R. J. Coupled-Cluster Methods with Non-iterative Triple Excitations for Restricted Open-Shell Hartree-Fock and Other General Single-Determinant Reference Functions. Energies and Analytical Gradients. *J. Chem. Phys.* **1993**, *98*, 8718-8733.

[36] Bartlett, R. J.; Musial, M. Coupled-Cluster Theory in Quantum Chemistry. *Rev. Mod. Phys.* **2007**, *79*, 291-352.

[37] Douglas, M.; Kroll, N. M. Quantum Electrodynamical Corrections to the Fine Structure of Helium. *Ann. Phys.* **1974**, *82*, 89-155.

[38] Jansen, G.; Hess, B. A. Revision of the Douglas-Kroll Transformation. *Phys. Rev. A* **1989**, *39*, 6016.

[39] Wolf, A.; Reiher, M.; Hess, B. A. The Generalized Douglas-Kroll Transformation. *J. Chem. Phys.* **2002**, *117*, 9215-9226.

[40] de Jong, W. A.; Harrison, R. J.; Dixon, D. A. Parallel Douglas-Kroll Energy and Gradients in Nwchem: Estimating Scalar Relativistic Effects Using Douglas-Kroll Contracted Basis Sets. *J. Chem. Phys.* **2001**, *114*, 48-53.

[41] Kendall, R. A.; Dunning, T. H., Jr.; Harrison, R. J.: Electron Affinities of the First-Row Atoms Revisited. Systematic Basis Sets and Wave Functions. *J. Chem. Phys*. **1992**, *96*, 6796-6806.

[42] Peterson, K.A.; Dunning, Jr., T.H.: Accurate Correlation Consistent Basis Sets for Molecular Core-Valence Correlation Effects. The second Row Atoms Al - Ar, and the First Row Atoms B - Ne Revisted. *J. Chem. Phys.* **2002**, *117*, 10548-10560.

[43] De Jong, W. A.; Harrison, R. J.; Dixon, D. A. Parallel Douglas–Kroll Energy and Gradients in NWChem: Estimating Scalar Relativistic Effects Using Douglas–Kroll Contracted Basis Sets. *J. Chem. Phys*. **2001**, *114*, 48-53.

[44] Rulin, F.; Peterson, K.A.: Correlation Consistent Basis Sets for Actinides. II. The Atoms Ac and Np – Lr. *J. Chem. Phys.* **2017**, *147*, 084108.

[45] Watts, J. D.; Gauss, J.; Bartlett, R. J. Coupled-Cluster Methods with Non-iterative Triple Excitations for Restricted Open-Shell Hartree-Fock and Other General Single-Determinant Reference Functions. Energies and Analytical Gradients. *J. Chem. Phys.* **1993**, *98*, 8718-8733.

[46] Deegan, M. J. O.; Knowles, P. J. Perturbative Corrections to Account for Triple Excitations in Closed and Open Shell Coupled Cluster Theories. *Chem. Phys. Lett.* **1994**, *227*, 321-326.

[47] Rittby, M.; Bartlett, R. J. An Open-Shell Spin-Restricted Coupled Cluster Method: Application to Ionization Potentials in N_2. *J. Phys. Chem*. **1988**, *92*, 3033-3036.

[48] Knowles, P. J.; Hampel, C.; Werner, H.-J. Coupled Cluster Theory for High Spin, Open Shell Reference Wave Functions *J. Chem. Phys.* **1993**, *99*, 5219-5228.

[49] Fang, Z.; Vasiliu, M.; Peterson, K. A.; Dixon, D. A. Prediction of Bond Dissociation Energies/Heat of Formation for Diatomic Transition Metal Compounds: CCSD(T) Works. *J. Chem. Theor. Comp.*, **2017**, *13*, 1057−1066

[50] Fang, Z.; Both, J.; Li, S.; Yue, S.; Aprà, E.; Keçeli, M.; Wagner, A. F.; Dixon, D. A. Benchmark Calculations of Energetic Properties of Groups 4 and 6 Transition Metal Oxide Nanoclusters Including Comparison to Density Functional Theory. *J. Chem. Theory Comput.* **2016**, *12*, 3689−3710

[51] Perdew, J. P.; Wang, Y. Accurate and Simple Analytic Representation of the Electron-Gas Correlation Energy. *Phys. Rev. B* **1992**, *45*, 13244-13249.

[52] Perdew, J. P.; Burke, K.; Wang, Y. Generalized Gradient Approximation for the Exchange-Correlation Hole of a Many-Electron System. *Phys. Rev. B* **1996**, *54*, 16533-16539.

[53] Burke, K.; Perdew, J. P.; Wang, Y. Derivation of a Generalized Gradient Approximation: The PW91 Density Functional in *Electronic Density Functional Theory: Recent Progress and New Directions*, Eds. Dobson, J.F.; Vignale, G.; Das M.P. Plenum, New York, 1997, pp. 81-122.

[54] Lee, T. J.; Taylor, P. R. A Diagnostic for Determining the Quality of Single-Reference Electron Correlation Methods. *Int. J. Quantum Chem. Symp.* **1989**, *23*, 199-207.

[55] Werner H.-J.; Knowles, P. J.; Knizia, G.; Manby, F. R.; Schütz, M.; Celani, P.; Györffy, W.; Kats, T.; Korona, T.; Lindh, R.; Mitrushenkov, A.; Rauhut, G.; Shamasundar K. R.; Adler, T. B.; Amos, R. D.; Bernhardsson, A.; Berning, A.; Cooper, D. L.; Deegan, M. J. O.; Dobbyn, A. J.; Eckert, F.; Goll, E.; Hampel, C.; Hesselmann, A.; Hetzer, G.; Hrenar, T.; Jansen, G.; Köppl, C.; Liu, Y.; Lloyd, A. W.; Mata, R. A.; May, A. J.; McNicholas, S. J.; Meyer, W.; Mura, M. E.; Nicklass, A.; O'Neill D. P.; Palmieri, P.; Peng, D.; Pflüger, K.; Pitzer, R.; Reiher, M.; Shiozaki, T.; Stoll, H.; Stone, A. J.; Tarroni, R.; Thorsteinsson, T.; Wang, M. MOLPRO, version 2015.1, a package of *ab initio* programs, See http://www.molpro.net.

[56] Werner H.-J.; Knowles, P. J.; Knizia, G.; Manby, F. R.; Schütz, M. Molpro: A General-Purpose Quantum Chemistry Program Package. *WIREs Comput. Mol. Sci.* **2012**, *2*, 242-253.

[57] Peterson, K. A. Correlation consistent basis sets for actinides. I. The Th and U atoms. *J. Chem. Phys.* **2015**, *142*, 074105(14 pages).

[58] Dolg, M; Cao, X. Accurate Relativistic Small-Core Pseudopotentials for Uranium and First Applications to Uranium Hydride. *J. Phys. Chem. A* **2009**, *113*, 12573-12581.

[59] Weigand, A.; Cao, X.; Hangele, T.; Dolg, M. Relativistic Small-Core Pseudopotentials for Actinium, Thorium, and Protactinium. *J. Phys. Chem. A.* **2014**, *118*, 2519-2530.

[60] Wang, T.-H.; Fang, Z.; Gist, N. W.; Li, S.; Dixon, D. A.; Gole, J. L. Computational Study of the Hydrolysis Reactions of the Ground and First Excited Triplet States of Small TiO_2 Nanoclusters. *J. Phys. Chem. C*, **2011**, *115*, 9344-9360

[61] Fang, Z.; Outlaw, M. D.; Smith, K. K.; Gist, N.W.; Li, S.; Dixon, D. A.; Gole, J. L. Computational Study of the Hydrolysis Reactions of Small MO_2 (M= Zr and Hf) Nanoclusters with Water. *J. Phys. Chem. C*, **2012**, *116*, 8475-8492

[62] Hammond, G. S. A Correlation of Reaction Rates. *J. Am. Chem. Soc.* **1955**, *77*, 334–338.

[63] Reed, A. E.; Curtiss, L. A.; Weinhold, F. Intermolecular Interactions from a Natural Bond Orbital, Donor-Acceptor Viewpoint. *Chem. Rev.* **1988**, *88*, 899-926.

[64] Weinhold, F.; Landis, C. R. *Valency and Bonding: A Natural Bond Orbital Donor-Acceptor Perspective*, University Press: Cambridge, U.K., 2005

[65] Glendening, E. D. ; Badenhoop, J. K.; Reed, A. E.; Carpenter, J. E.; . Bohmann, J. A; Morales, C. M.; Landis, C. R.; Weinhold, F. Natural Bond Order 6.0, Theoretical Chemistry Institute, University of Wisconsin, Madison, WI, 2013.

[66] Glendening, E. D.; Landis, C. R.; Weinhold, F. NBO 6.0: Natural Bond Orbital Analysis Program. *J. Comp. Chem.* **2013**, *34*, 1429-1437.